Simulating SEM imaging of via bottoms

Benjamin D. Bunday[a], Chris Mack[b], Shari Klotzkin[c], Douglas Patriarche[d], Yvette Ball[a]

[a]AMAG nanometro, Schenectady, NY, 12303, USA
[b]Fractilia, Austin, TX, 78703, USA
[c]AMAG nanometro, Binghamton, NY, 13850, USA
[d]AMAG nanometro, Ottawa, ON, K2G 5M9, Canada

ABSTRACT

Scanning electron microscope (SEM) imaging is widely used in semiconductor manufacturing, including for defect inspection. One use is to identify contact holes that are potentially scummed (not completely cleared to the substrate). However, the visibility of the bottom of a contact hole (and thus the ability to identify scumming) is limited when the aspect ratio of the hole becomes high. In this work, a large designed experiment simulation study using AMAG SimuSEM will thoroughly explore the parametric influences of profile and CD for via bottom detection in the secondary electron regime, including not only aspect ratio, but also influences of sidewall angle and footing, along with defect cases of incomplete etch or resist residues in hole bottoms. We will show the expected trends to the signal evolution as a function of the applied perturbations, and demonstrate that simulation can be used to understand and estimate the thresholds for detecting via footing and scumming.

Keywords: CD-SEM, JMONSEL, SimuSEM, via, contact, computational SEM, Monte Carlo simulation, SEM simulation

1. INTRODUCTION

Scanning Electron Microscope (SEM) imaging of via / contact hole samples is a key application case of importance requiring accurate 3D critical dimension (CD) metrology. These vias are themselves crucial common components in integrated devices, requiring precise inspection and characterization to ensure yield. SEM allows for high-resolution imaging, enabling researchers to scrutinize via structures at the nanoscale, measuring dimensions, identifying defects, or assessing material properties. Both lithography and etches of these features, considered especially critical for memory and logic cases, are APC (Advanced Process Control)-controlled by these measurements. Therefore, product quality is strongly dependent on achieving tight feature-to-feature size and placement distributions. Key issues in SEM imaging of via samples include the need for optimized imaging parameters to achieve the desired resolution while avoiding damage to the sample. Additionally, understanding the electron-beam-sample interaction and interpreting SEM images accurately are vital aspects to overcome when studying via samples. Subtle 3D profile details of vias such as top corner rounding, sidewall angle, sidewall bowing, footing, or in more severe cases hole bottoms with residual plugs of photoresist or incomplete etch to intended depth, can be important so that the profile shape and detected bottom are of main interest for measurement for process control and to detect such process excursions.

In this work, a large designed experiment simulation study will thoroughly explore the parametric influences of profile and CD for via bottom detection in the secondary electron (SE) regime. As known in practice, the effect of aspect ratio is the primary factor in the capability to detect a via bottom, and this basic dependence is the core case simulated. In addition to exploring aspect ratio, which inherently includes depth and hole CD, the influences of sidewall angle and footing will be explored, along with defect cases of incomplete etch or resist residues in hole bottoms. Beam energy will also be varied within the DOE, among 300 V, 500 V and 800 V values, exploring the DOE with both SiO_2 on Si and PMMA on Si structures. This study is performed using the SEM simulation software AMAG SimuSEM [1-2], based on NIST's JMONSEL [3-19], which makes possible the SEM design of experiment (DOE) simulation experiments. The main goal of the work will be to answer the question, under what circumstances will a top-down CD-SEM reliably detect the presence of scumming at the bottom of a contact hole? The use of simulation DOEs to predict best conditions and performance for the above applications will be demonstrated.

2. SEM SIMULATIONS

To fabricate in the nanoscopic size regime, one must be able to competently image and measure what is being built. Thus, the importance of improved metrology continues to grow as Moore's Law progresses and devices continue to shrink, become more complex with multiple layers and new include materials. Scanning Electron Microscopes (SEMs) image physical samples using scanning electron beams—electrons raster across solid objects and collect intensity/energy versus position information to form maps showing surface structure with possibly some depth information measuring backscattered electron yields.

SEM measurements are crucial in R&D and manufacturing of semiconductor chips. However, these types of measurements are very expensive, and simulation support helps chip manufacturers achieve measurements that improve manufacturing yield, are statistically significant enough to make process decisions, and save time and money accelerating development of next generation chips. SEM simulation capability will contribute to the metrology understanding necessary during IC device fabrication, both during development of new devices and manufacturing process control. The tightness of the distribution of widths of billions of transistors on a chip is only producible to tolerance with the appropriate process monitoring.

SEM metrology is the main workhorse technique for a fab's process control, and a fab's eyes to yield-killing defectivity. These tools are operating near resolution and speed limits, such that simulation support for understanding the measurements and images is critical to successful, constructive and stable metrology. SEM imaging and electron beam condition optimization is important for achieving the best signal to noise possible of the aspect of the feature under evaluation, and this optimum is very sample-type and condition dependent. Additionally, if exploring items not easy to build at time of interest, as is the case when process development begins, simulation is an inexpensive alternative to tailor-building tools to explore a trial condition, or have built to perfection applicable samples for physical imaging case studies, including preliminary studies on samples which might be items possible years in future but cannot be built very well at present. Simulation allows conclusive results for such studies due to the full knowledge of the user-defined sample, and at a very small fraction of the cost or time involved for physical experiments. Once validated, a SEM simulation model can be used to extrapolate similar imaging to mass produce images over an entire process window, which can be effective for dealing with models involving larger parameter spaces. Simulation thus allows predictions to target other efforts, along with other advantages such as tailored model-based algorithms to measure a given case of interest, which will be necessary to maintain accurate and precise measurements of features of sizes close to resolution limits at 5 nm and 3 nm nodes and beyond. Also, such simulations can be used to produce images for other purposes such as calibrating AI image analysis tools with faux images, studying the evolution of 2D shape contours of different features at different conditions, or for providing a standard for comparison to other metrologies through physical data or comparison of simulation results. Also, SEM simulations are used to determine best SEM conditions for measurement or imaging of various applications, or understand issues in measuring various feature types. Recently, the advent of High Voltage SEM (HV-SEM) becoming mainstream fab tools has enabled the ability to calibrate optical overlay with see-through SEM imaging, and simulators are valuable for understanding needed beam conditions to detect desired buried signals for different applications. SEM simulation is crucial for understanding the SEM metrology best practices, conditions and error sources which influence the success of metrology in such efforts.

SEM simulation software used

SEM simulator software has been available for ~20 years, starting with NIST's MONSEL. Its Java sequel, NIST's JMONSEL, **J**ava **MON**te Carlo **S**imulator for **S**econdary **EL**ectrons, is a 3D electron beam simulation software package developed and programmed in the 2010-12 timeframe at National Institute of Standards & Technology (NIST) by Dr. John Villarrubia, and funded by SEMATECH AMAG. The purpose of the program was to enable limits simulation studies for defect and critical dimension SEM metrology. NIST has supported ongoing improvement and validation efforts since, and it is now well validated for non-charging cases, with some use by a small user community.[3-19] SimuSEM is a fully integrated simulation software package with over 40 well documented materials which uses the rigorously validated physics of JMONSEL to compute electron trajectories and electron material interactions, transforming JMONSEL into an integrated computational SEM simulation package, ready to deploy now on industrial-scale complex problems by calculating DOEs spanning entire geometric process windows of parameterized structures, with large flexibility to adapt to any case, and with a GUI allowing the user to be productive within days for significant work. SimuSEM's material

models are constantly expanding and will be automatically compatible with new upcoming materials models from the NIST Physical SE Yield Laboratory, coming soon, which will enable materials definitions of any material in modern apples-to-apples NIST characterizations done with the latest sample preparation technology, allowing much more accurate materials models, even for proprietary samples.

JMONSEL uses a Monte Carlo simulation to track primary electrons as they enter a material, scatter, lose energy, and generate secondary and backscattered electrons. By monitoring the electrons that exit the material and are captured by a detector (software counter element), the electron yields can be found at any point designated as a target pixel. The physical models in JMONSEL are the best-known models in the literature in the energy ranges used here, are open-source, with complete transparency in their documentation, definition, implementation, and execution, as programmed by NIST, with thirteen years of validation data and wide acceptance by the industry.

```
# Layer.s3
    location = [  0.000*meterspernm,  0.000*meterspernm,557.500*meterspernm]
    rotation = [  0.000*math.pi,  0.000*math.pi,  0.000*math.pi]
    dimensions = [500.000*meterspernm,500.000*meterspernm, 15.000*meterspernm]
    thickness3=location[2]+dimensions[2]/2
    layers3=mon.NormalMultiPlaneShape()
    layers3.addPlane(normalVector,[0,0,thickness2])
    layers3.rotate(location,-math.pi/2,rotation[0],math.pi/2)
    layers3.rotate(location,0,rotation[1],rotation[2])
    layers3region = monte.addSubRegion(layers2region,SiMSMDeep,layers3)
```

Figure 1: example few lines for describing a feature in a conventional pre-SimuSEM JMONSEL script which can be as long as 1000 lines of rigorous math and spatial relationships, with no means for visualization of the target other than trial and error which is very cumbersome and time-consuming, and with the extreme detail involved complex features are very challenging to define, if not practically impossible.

However, the primitive JMONSEL code does have shortcomings. The largest of these is lack of user-friendliness. Gaining proficiency with the primitive JMONSEL code takes much time with a steep and long learning curve, and the sample definition functions, while simple at a basic level, can become extremely complex to visualize for the programmer when trying to design features of the complexity of modern-day device structures or any 3D shapes beyond a few basic included shape primitives, impractical to code on a large scale for complex features. It had only minimal visualization thru VRML viewed in a web browser, no graphical interface. Original JMONSEL required very rigorous, involved, detailed line-edited Jython scripts, that typically would be 600-1000 lines long or more, and were themselves full Jython programs that called up core JMONSEL functions. See Figure 1 of a small part of a Jython script to just define part of the substrate. Another shortcoming of original JMONSEL was that it was not speed optimized; small images would take hours, and large projects could take days or months, especially when charging was attempted which ran so slow it was deemed impractical. Old JMONSEL had issues with sometimes pixel times increasing with number of pixels such that larger jobs would gradually bog down and take very long to finish near the end.

SimuSEM is a greatly accelerated, user-friendly, mature version of JMONSEL with rich and reliable visualization. SimuSEM uses JMONSEL as its core physics and addresses JMONSEL's shortcomings by greatly improving the simulation run speed and providing a user-friendly front-end GUI and tools to visualize and analyze the results. SimuSEM, which includes many original improvements to JMONSEL, includes a modern intuitive 3D graphical GUI which makes the code much more usable. This program provides the user with greatly improved utility, productivity, flexibility, visualization, accessibility, and achievable complexity of designed features while improving simulation speed and scalability, plus many other refinements and additions, and superior results access. Additionally, the new code allows viewing of all electron trajectories in the 3D environment and other nanoscopic views of the results. Thus, additional observations on how various process subtleties might affect the SEM signal can be studied. See Figure 2 for comparison to Figure 1 to see how all JMONSEL functionality is now built into Blender.[20] All features are now reduced to best practices based on much experience using the code by the authors, who have built the SimuSEM GUI with accessibility to features and sample and results visualization as priorities.

Speed optimization of JMONSEL also got a major overhaul as a major targeted improvement, so in this project these issues have been addressed and the runtime simulation speed optimized >35x for a single core but with multithreading added, >5000x faster than original JMONSEL with confirmed unchanged outputs, and with the pixel time slowdown issue eliminated. Another past shortcoming of JMONSEL which SimuSEM addresses with much improvement is the materials library—SimuSEM includes many new defined materials and the ability to add more with basic material information and with a few points of SE yield data, and also is expandable in future as NIST is bringing up a new material electron yield

characterization laboratory which will output everything needed to produce new materials definitions from experimental samples.[21]

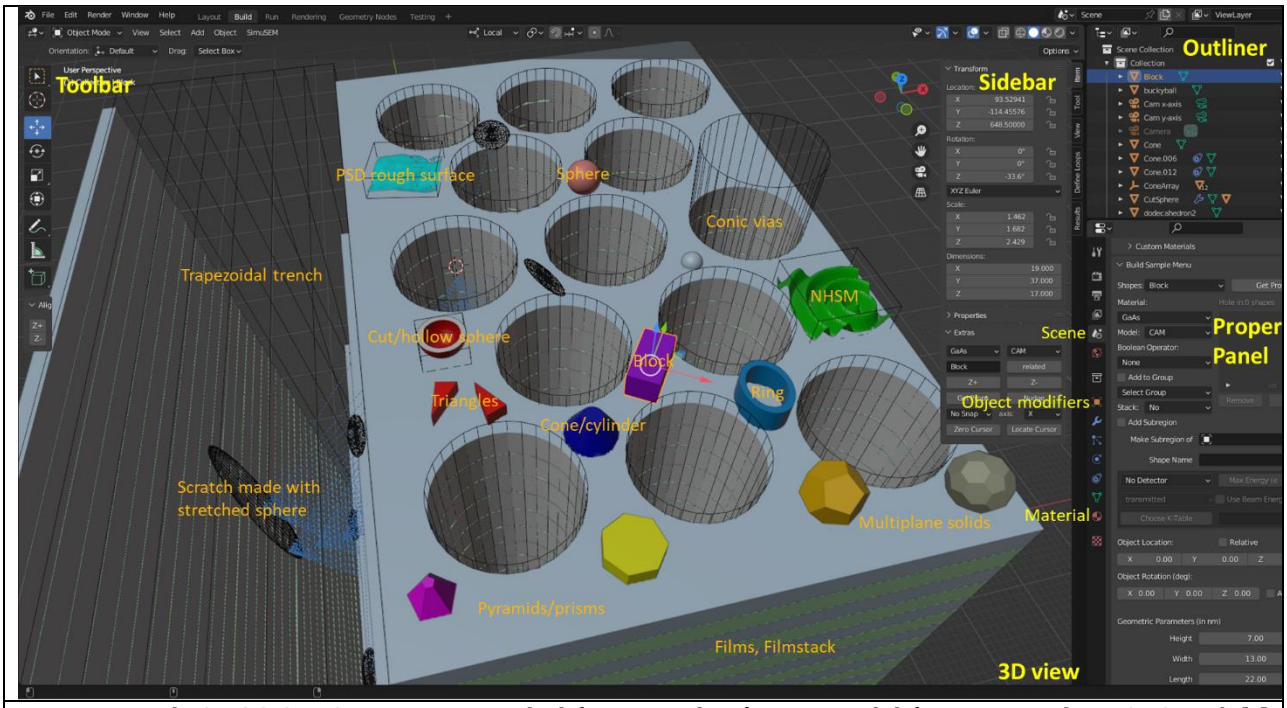

Figure 2: Example AMAG SimuSEM intuitive sample definition window for intentional defect array sample on ONO stack [2] augmented with many different example structures. The GUI allows full 3D visualization at any scale or angle including see-thru mode, a good set of ready-to-use shape types, simple mouse-driven modification and many best JMONSEL practices and features plus new features with SimuSEM, with all routines built into a systematic package making all capabilities commonly available and ready for user deployment, including parametric loop definition for large scale DOEs.

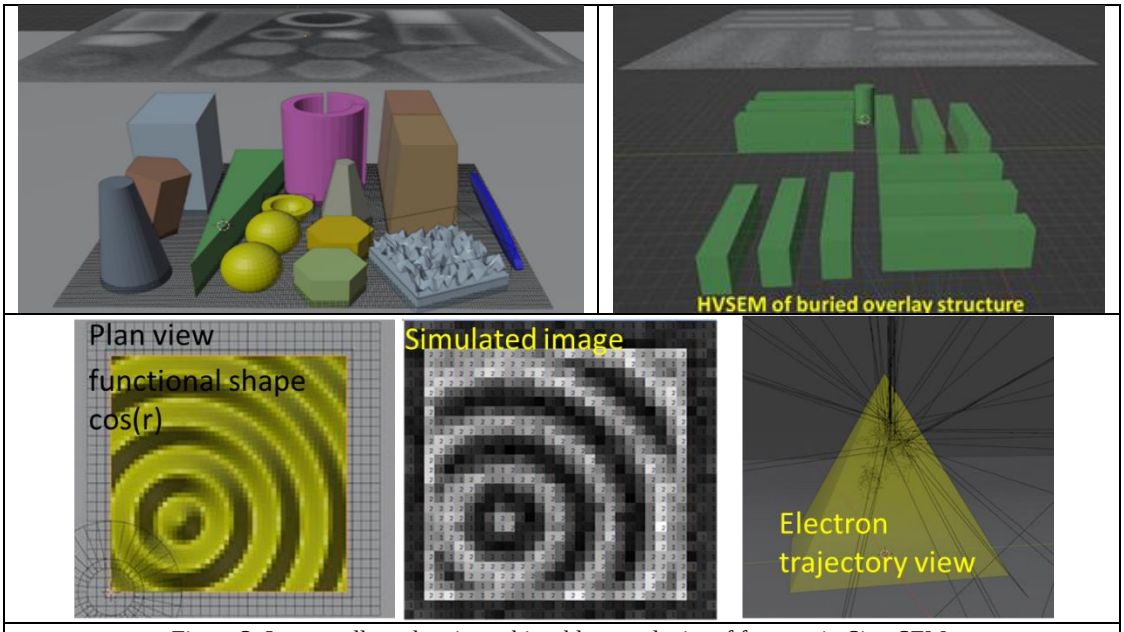

Figure 3: Image gallery showing achievable complexity of features in SimuSEM.

With the previously mentioned improvements, SimuSEM can address many more simulation cases with much more complexity as required for contemporary needs. Figures 2 and 3 show some more example images of achievable complex features using SimuSEM.

Simulation DOEs in this study

The main goal of this work is to answer the question, under what circumstances will a top-down CD-SEM reliably detect the presence of scumming at the bottom of a contact hole? To address this, we do a DOE study to explore scumming and footing in SiO_2 on Si and PMMA on Si. First we simulate the 4D DOE of SE signal across conic holes for height, diameter, sidewall angle and beam energy, for both SiO_2 and PMMA cases. From this main DOE of the basic conic via cases, we will find the central DOE condition to further explore footing and scumming. At that central setting for the basic hole dimensions, we then simulate a conic foot in the base of hole, and films stacked in bottom of hole, to explore footing and scumming.

The main simulation DOE is a full factorial of conic contact hole, in both SiO_2-on-Si and PMMA-on-Si, varying CD_{bot} = 15 to 60 nm step 5 nm, hole height h = 10 to 100 nm step 10 nm, sidewall angle (SWA) = 0° to 10° step 5°, and V_{acc} = 300 V, 500 V, 800 V. A total of 900 linescans were simulated thru the DOE. Pixel size was 0.5 nm with N = 5000 trajectories per pixel. See figures 4 and 5 to visualize the DOE.

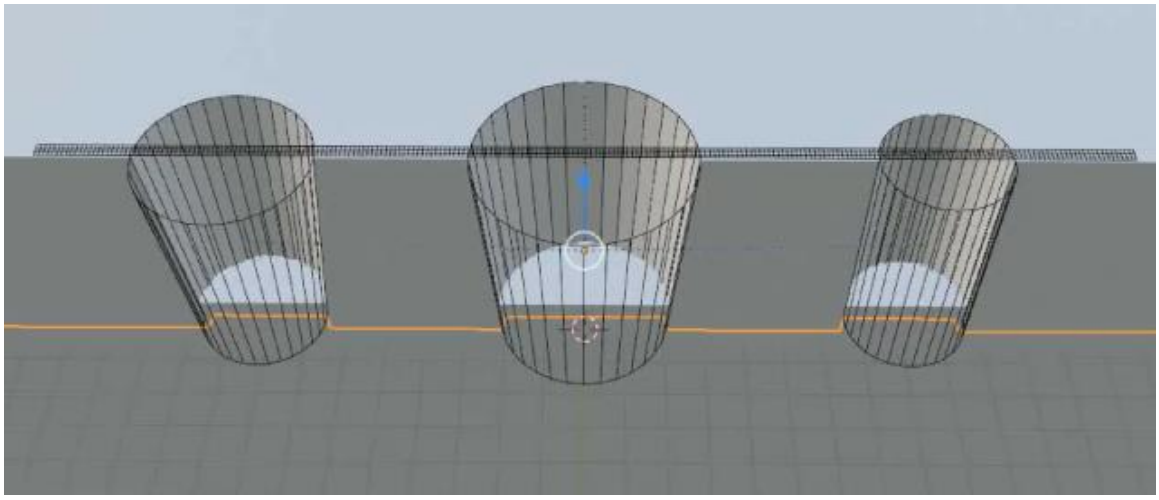

Figure 4: 3D view in SimuSEM of three holes with the different sidewall angles used in the DOE, on left 5°, center 10°, and right 0°. The actual recipe had one single conic hole looping bottom CD, height, and SWA, plus beam energy.

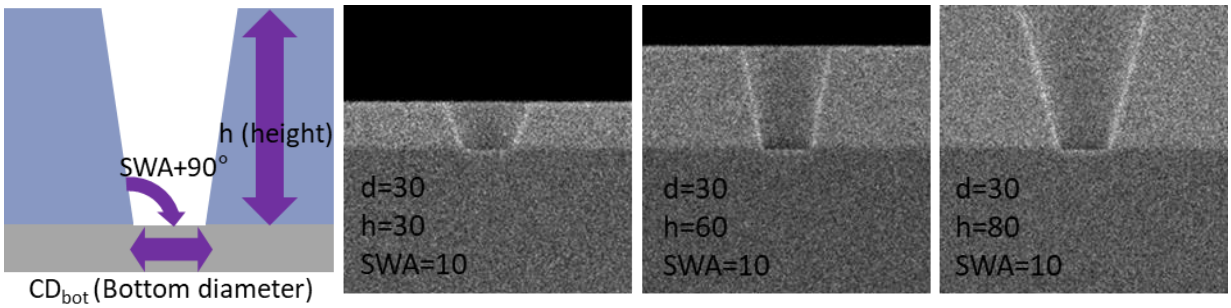

Figure 5: Main via DOE. Left: Diagram showing the varying geometric parameters. Right three images: Example cross-section SEM simulations of the achieved profiles to verify target, of different via depths at a single SWA and CD. Note SWA is defined from the vertical, but shown here as SWA+90° from the horizontal.

Example results from this main DOE are shown below, and from those we chose a central condition of typical interest to conduct further DOE studies of footing and scumming. This central condition was chosen to be the vias with 30 nm diameter and 60 nm height hole, with aspect ratio of 2. At this condition, we vary the main hole SWA and beam energy, but fix height and CD. Note, we define aspect ratio (AR) as height/bottom CD.

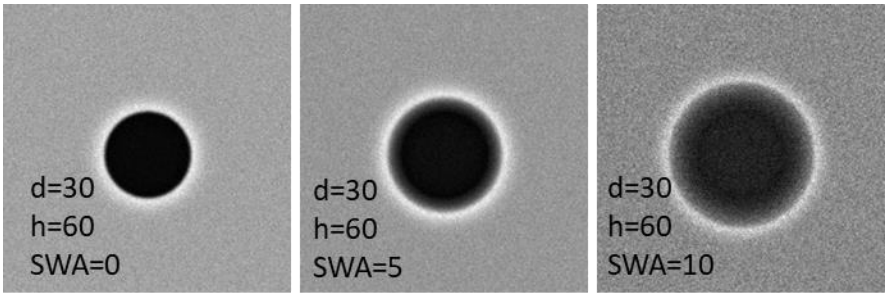

Figure 6: Example full images of the central condition at the different SWA values, with 0.5 nm pixels and N = 500 trajectories.

To explore footing at the via base, a DOE varying the SWA of a shallow conic foot of height 5 nm at the base of the hole was simulated, with SWA_{hole} = 0° to 10° step 5°, SWA_{foot} = 0° to 70° step 5°, and V_{acc} = 300 V, 500 V, 800 V. These were run at N=1000 trajectories and 0.5 nm pixels.

To explore varied films in hole bottom (scumming), the AR=2 hole is partially filled at the bottom with films of the given material, with scum depth = 0 to 30 nm step 5 nm, SWA_{hole} = 0° to 10° step 5°, and V_{acc} = 300 V, 500 V, 800 V. These were run at N=1000 trajectories and 0.5 nm pixels.

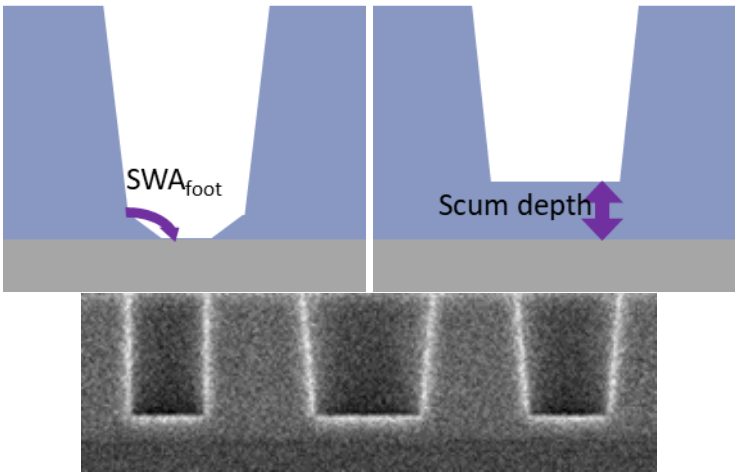

Figure 7: Footing and scumming DOEs. Left: Diagram showing the varying geometric parameters of the foot DOE. Center: Diagram showing the varying geometric parameters of the scumming DOE. Right: Example cross-section SEM simulation of the achieved profiles to verify target, of different scumming depths at a single CD at all three SWA values, in this case the 60 nm depth hole had 10 nm of scumming film in via bottom.

Figure 8 shows example results from the main DOE of via AR for SiO_2 on Si. Showing the entire DOE is space prohibitive, but these are representative results. Deeper holes, as expected, suppress the signal from hole bottom and thus show lower SE yield, and plotting these average SE yields leads to an exponential decay trend which will be modeled in the next section. Figure 9 shows the results for the footing DOE for both SiO_2 on Si and PMMA on Si. Note that the signal from bottom varies only slightly and is likely "in the noise" so the effect of footing is minimal and will not change the CD measurement.

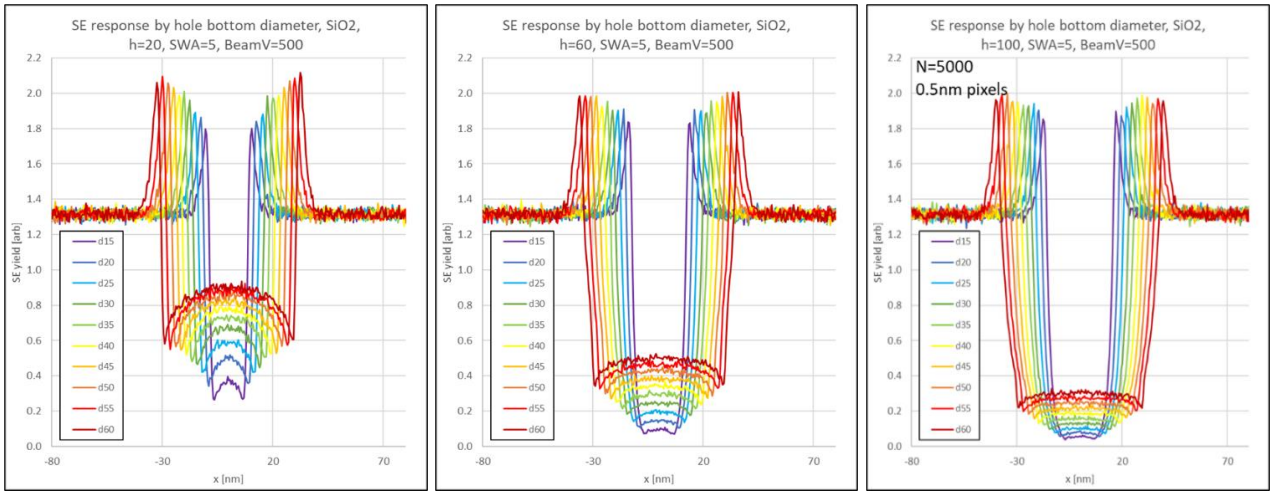

Figure 8: Example results from main via DOE, with each graph showing a single via depth at SWA = 5° and Beam V = 500 V, and with each curve showing the SE yield response across the via at a different diameter of bottom CD (each diameter hole denoted as d in the legend).

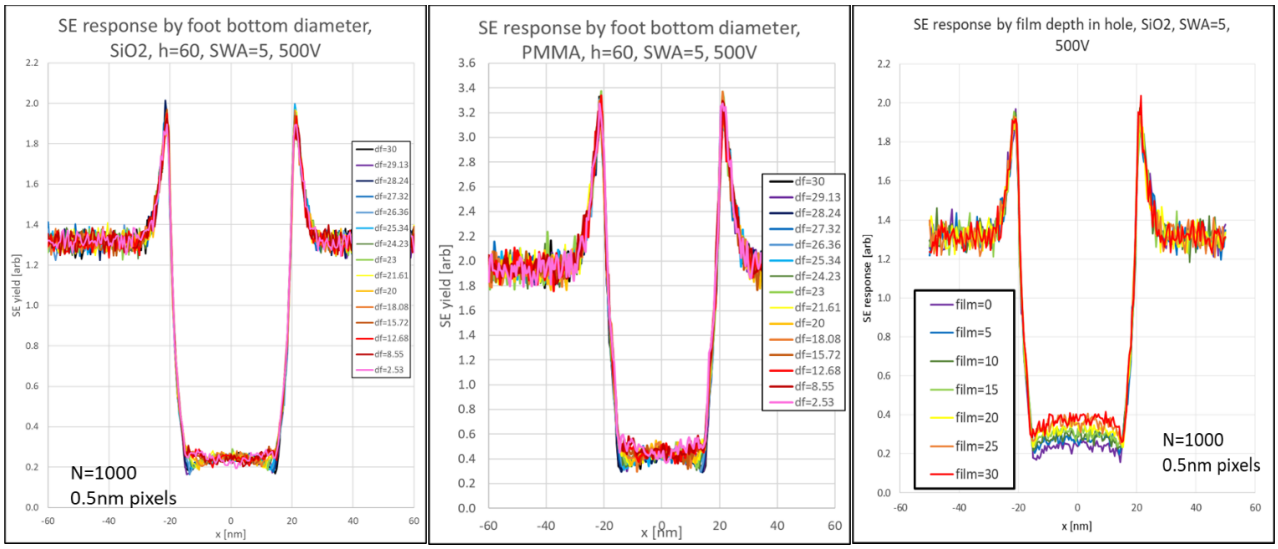

Figure 9: Left: Results from footing DOE for SiO_2 on Si case. The foot was varied as a SWA_{foot} but in the graph each foot condition is denoted by df, which is the diameter of the foot opening at the center of the via; the foot was 5 nm high at the hole edge. Very little response is observed. Center: Same graph for PMMA on Si case. Right: Results for SiO_2 on Si for scumming film depths from 0 to 30 nm.

The above results are thoroughly quantitatively summarized and analyzed in the next section.

3. MODELING ASPECT RATIO BEHAVIOR

One of the goals for these SEM simulation results is to understand the roles of feature geometry and SEM conditions on the visibility of the bottom of the contact hole. To that end, the data was analyzed by finding an average SEM signal value in the center of the hole, and also an average SEM signal value in the background region, away from the hole, for each condition. In Figure 10, the ratio of these two values is plotted versus the aspect ratio of the hole (feature height divided by bottom width) for the case of a SiO_2 hole on a silicon substrate. Three different SEM voltages (landing energies) are

shown, and in each plot are data from holes with three different sidewall angles (SWA, in degrees, with 0 = vertical profile). The data are for a matrix of ten different hole diameters (from 15 nm to 60 nm) and ten different hole heights (from 10 nm to 100 nm). Figure 11 shows the same plots for the case of PMMA on silicon.

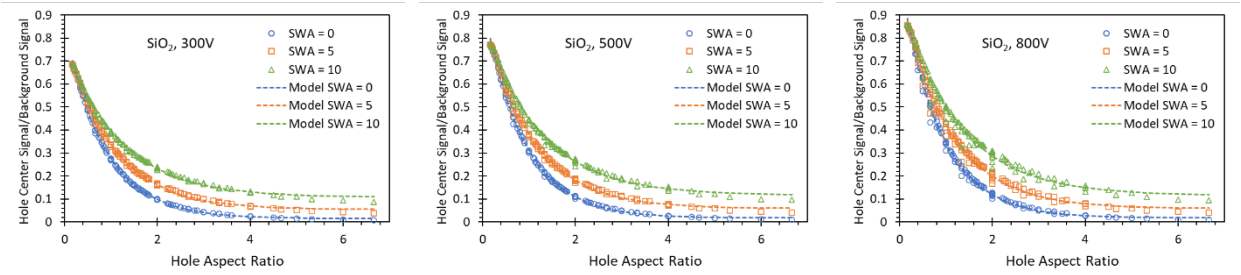

(a) (b) (c)

Figure 10. Plot of the simulated hole center to background signal versus hole aspect ratio (symbols) for three different voltages for the case of SiO_2 features on Si: (a) 300 V, (b) 500 V, and (c) 800 V. Each graph also shows three different sidewall angles (SWA, in degrees). The dashed lines represent the best fit of the aspect ratio model to each data set.

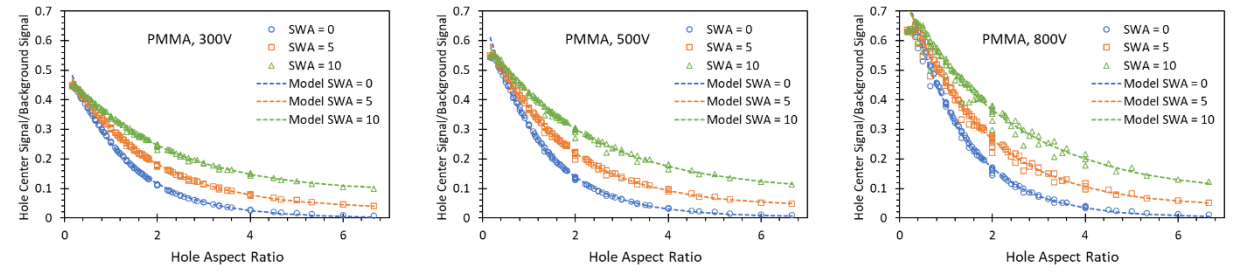

(a) (b) (c)

Figure 11. Plot of the simulated hole center to background signal versus hole aspect ratio (symbols) for three different voltages for the case of PMMA features on Si: (a) 300 V, (b) 500 V, and (c) 800 V. Each graph also shows three different sidewall angles (SWA, in degrees). The dashed lines represent the best fit of the aspect ratio model to each data set.

It is clear that the aspect ratio is the controlling geometric factor in terms of the signal escaping from the bottom of the hole in all cases, rather than hole diameter and height individually. A simple exponential model fits the data quite well in all cases.

$$y = Y_0 e^{-AR/\eta} + Y_\infty \qquad (1)$$

where y is the ratio of the hole center signal to the background signal and AR is the hole aspect ratio. The best first model parameters for silicon dioxide holes on a silicon substrate are given in Table I, with the PMMA on silicon results in Table II. As the graphs in Figures 10 and 11 show, this model fits the data extremely well in all cases. It is interesting to note that for silicon dioxide, the three sidewall angle curves always cross at an aspect ratio of 0.2 for each voltage. For PMMA, the three sidewall angles cross at $AR = 0.3$ for each voltage. The y value at this crossing point is voltage dependent, but not sidewall angle dependent.

It is interesting to plot the model parameters η and Y_∞ versus voltage and sidewall angle. Figure 12 shows these model parameters for the case of PMMA holes on silicon, but similar results are seen for SiO_2. To first order it is clear that these parameters are controlled by the geometric factor sidewall angle, and have very little dependence on voltage. Thus, the

model can be broken down into terms that are geometry dependent but not voltage dependent (η and Y_∞) and a term that is voltage dependent but not geometry dependent (Y_0, or more exactly the y value at which the curves cross).

Table I. Best-fit model parameters for the case of SiO_2 holes on silicon.

Voltage	SWA	Y_0	η	Y_∞
300V	0°	0.548	1.269	0.003
	5°	0.483	1.723	0.030
	10°	0.414	2.243	0.077
500V	0°	0.694	1.223	0.004
	5°	0.608	1.650	0.039
	10°	0.524	2.201	0.090
800V	0°	0.864	1.215	0.002
	5°	0.761	1.668	0.036
	10°	0.680	2.336	0.077

Table II. Best-fit model parameters for the case of PMMA holes on silicon.

Voltage	SWA	Y_0	η	Y_∞
300V	0°	0.548	1.269	0.003
	5°	0.483	1.723	0.030
	10°	0.414	2.243	0.077
500V	0°	0.694	1.223	0.004
	5°	0.608	1.650	0.039
	10°	0.524	2.201	0.090
800V	0°	0.864	1.215	0.002
	5°	0.761	1.668	0.036
	10°	0.680	2.336	0.077

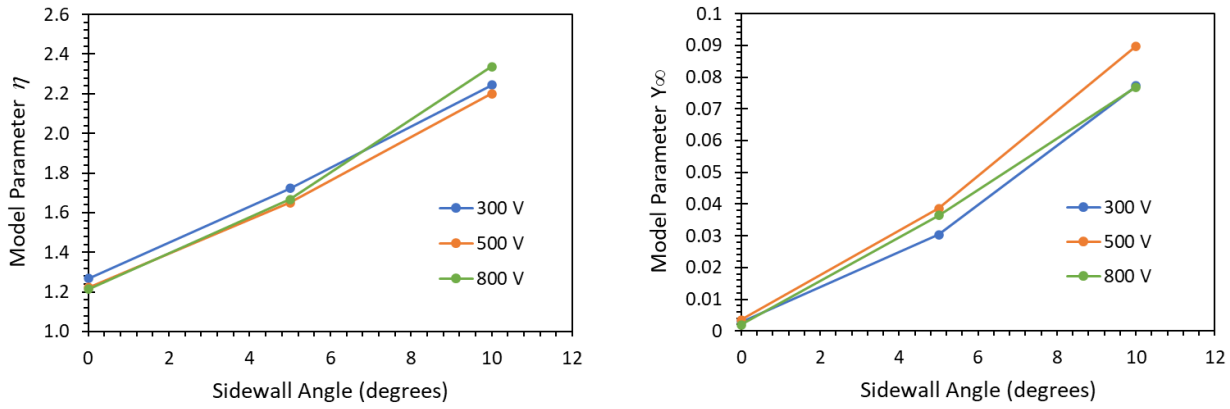

(a) (b)

Figure 12. Best-fit model parameters for the case of PMMA holes on silicon, shown as a function of voltage and sidewall angle.

Further SEM simulations were performed for the cases of a SiO_2 hole on a SiO_2 substrate and PMMA holes on a PMMA substrate. These conditions more closely resemble the case of a hole that has not completely cleared to the substrate (that is, a "scummed" hole). The behavior in these cases also follows the trends described above. Table III shows the model fit results for the case of PMMA holes on a PMMA substrate.

Table III. Best-fit model parameters for the case of PMMA holes on a PMMA substrate.

Voltage	SWA	Y_0	η	Y_∞
300V	0°	1.144	0.953	0.035
	5°	1.030	1.072	0.116
	10°	0.893	1.120	0.230
500V	0°	1.136	1.052	0.000
	5°	1.015	1.022	0.126
	10°	0.873	1.119	0.226
800V	0°	1.095	0.938	0.034
	5°	0.989	1.000	0.127
	10°	0.822	1.168	0.216

4. DETECTING CONTACT HOLE SCUMMING

One interesting use of the above SEM simulation results is to understand the capabilities of a SEM for detecting a hole that is scummed. One can think of a scummed hole (for example, where the hole only penetrates 50% through the film) as a hole with a lower aspect ratio (for example, 2X smaller). Using the exponential model above, we can predict the rise in the relative center signal of the hole as a function of the amount of scumming. For a set of SEM images containing many nominally identical holes, those holes can be measured to produce a mean grayscale level for the center of the holes (μ_{gc}) and a mean background grayscale level (μ_{gb}), so that the mean y value would be $y = \mu_{gc}/\mu_{gb}$. A reasonable detector for scummed holes would be to look for any hole with a relative grayscale value that is a set amount higher than this average.

SEM images, however, tend to be noisy, and so there is statistical uncertainty in the measured center grayscale value. If many holes are measured, both the mean center grayscale value and the standard deviation of the center grayscale values (σ_{gc}) can be measured. Figure 13 shows a typical distribution of center grayscale values. In this case, μ_{gb} = 155 (where the grayscale values range from 0 – 255), μ_{gc} = 65.3, and σ_{gc} = 4.5.

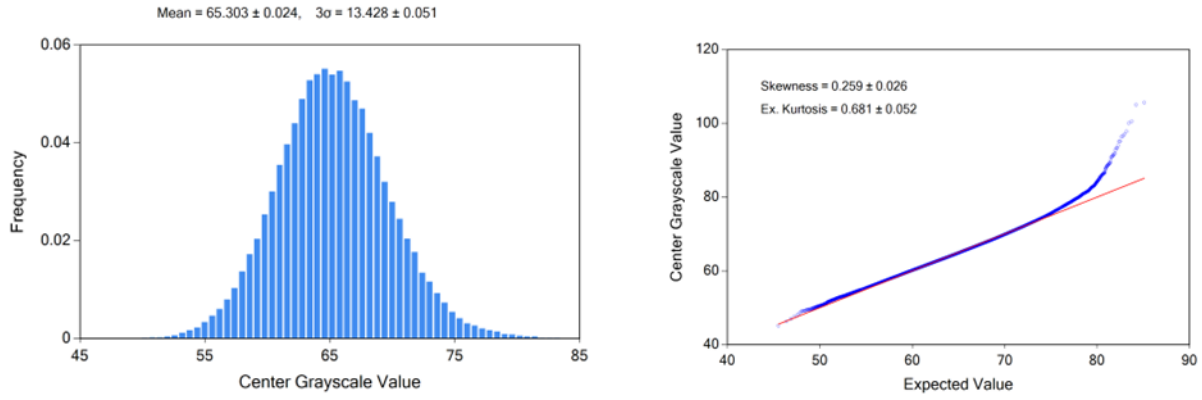

Figure 13. The measurement of many contact holes yields a distribution of center grayscale value, with data plotted as (a) a histogram, and (b) a normal probability plot (the straight line indicates Gaussian behavior of the distribution). All data measured with MetroLER v4.2.0.

From Figure 13, it is clear that most of the contact hole center grayscale values follow a Gaussian distribution, but that the distribution is skewed, with some holes exhibiting higher than expected center grayscale levels. A reasonable choice for setting the criterion of when to call a hole scummed (or more descriptively, "potentially scummed") would be when the center grayscale value of any hole exceeds $\mu_{gc} + n\sigma_{gc}$. The choice of the value of n defines a trade-off between the sensitivity of the detector (what is the smallest amount of scumming that can be detected) and the number of false positives. The probability of a false positive can be determined assuming a Gaussian distribution of center grayscale values in the absence of scumming. For example, n = 4 results in 1 false positive per 30,000 contact holes. Increasing n reduces the false positive rate exponentially.

The sensitivity of the detector as a function of n can be determined using our exponential model. We can define the *Relative Scumming Detection Limit* as the smallest fraction of the hole that can be filled while still being reliably detected as scummed. After some algebra,

$$Relative\ Scumming\ Detection\ Limit = \frac{ln\left(1 + \frac{n\sigma_{gc}}{\mu_{gc} - \mu_{gb}Y_\infty}\right)}{ln\left(\frac{\mu_{gb}Y_0}{\mu_{gc} - \mu_{gb}Y_\infty}\right)} \qquad (2)$$

Interestingly, this limit is a function of Y_0 and Y_∞, but not η. Consider the data presented in Figure 13 and the modelled PMMA hole behavior detailed in Table III. For the case of 500 V and a sidewall angle of 5° we find that

$$\frac{\sigma_{gc}}{\mu_{gc} - \mu_{gb}Y_\infty} = 0.0988 \ \ and \ \ ln\left(\frac{\mu_{gb}Y_0}{\mu_{gc} - \mu_{gb}Y_\infty}\right) = 1.24 \qquad (3)$$

The impact of n on this detection limit is shown in Figure 14. Since the actual sidewall angle corresponding to the experimental data of Figure 8 is not known, three different sidewall angles were assumed. For n = 4, the smallest amount of scumming that can be reliably detected is about a 25 – 30% filled hole (depending on the actual sidewall angle). Note that the detection limit scales about linearly with n, but the false positive rate decreases exponential as n increases.

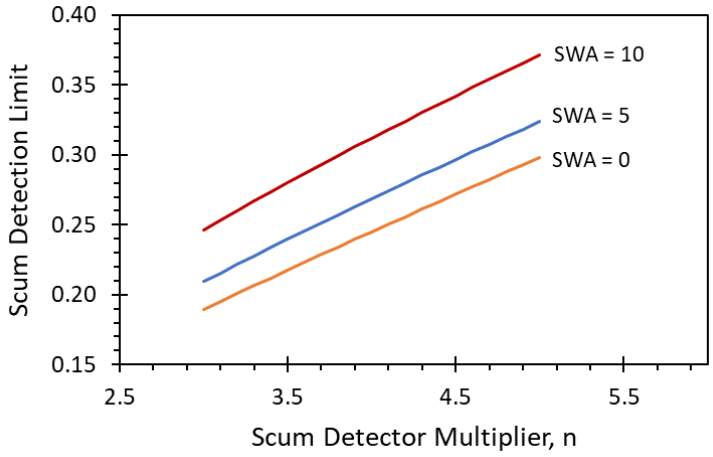

Figure 14. The Relative Scumming Detection Limit as a function of the multiplier n for the case of the data presented in Figure 13 and the modelled PMMA hole behavior detailed in Table III at 500 V and a sidewall angle of 5°.

5. CONCLUSIONS

One key finding of this work is that the scumming of significant depth of a hole is not nearly as visible under SEM as many previously believed. The SimuSEM via foot DOE demonstrated that a 5 nm foot at hole bottom is barely discernable

in our broad DOE at AR=2. Future work will be to confirm at more shallow AR. Deeper AR will give same answer as the signal gets more and more limited from such depths.

As seen above, geometric considerations control the via bottom signal. Aspect Ratio and sidewall angle are the main controlling components. For all of the combinations of materials and voltages, the aspect ratio alone (rather than feature width or height individually) determines the visibility of the hole bottom. Sidewall angle also impacts bottom hole visibility in a geometric way, with a shallower sidewall allowing more electrons to escape from the bottom of the hole. The simulations show that the rate of hole bottom signal decrease with increasing aspect ratio is not voltage dependent (over the range of voltages studied here).

When detecting scum, there is a tradeoff between false positives and sensitivity. We can define a "potentially scummed" hole as any hole whose center grayscale level exceeds the mean central grayscale value for all the holes plus a multiple of their standard deviation (a feature implemented in the MetroLER software). Detection sensitivity varies about linearly with the standard deviation multiplier n, yet false positives vary exponentially with n. A combination of modelling plus measurement can quantify this tradeoff. In this example, we were sensitive to 25-30% scumming in a resist hole with 1 in 30,000 false positive rate (n = 4).

More broadly, a computational SEM with an ability to run large parametric DOEs was demonstrated to be a valuable tool for generating the theoretical responses to make informed decisions when choosing strategies for deployment in real fab applications.

6. ACKNOWLEDGEMENTS

We would like to thank Dr. John Villarrubia of NIST for JMONSEL and all the years of development, evolution and support, and Dr. Andras Vladár of NIST for related discussions.

7. REFERENCES

[1] Bunday, Benjamin D., Klotzkin, S., Patriarche, D., Mukhtar, M., Maruyama, K., Kang, SK, Yamazaki, Y. "Simulating process subtleties in SEM imaging". Proceedings Volume 12053, Metrology, Inspection, and Process Control XXXVI; 120530A (2022) https://doi.org/10.1117/12.2615753 .

[2] Bunday, Benjamin D., Klotzkin, S., Patriarche, D., Mukhtar, M., Maruyama, K., Kang, SK, Yamazaki, Y. "Simulating HV-SEM imaging of HAR and buried features". Proceedings Volume 12496, Metrology, Inspection, and Process Control XXXVII; 124960W (2023) https://doi.org/10.1117/12.2661179 .

[3] Liddle, J. A., Hoskins, B. D., Vladár, A. E. and Villarrubia, J. S. "Research Update: Electron beam-based metrology after CMOS", APL Materials 6, 070701 (2018); https://doi.org/10.1063/1.5038249 .

[4] J.S. Villarrubia, et al., "Scanning electron microscope measurement of width and shape of 10 nm patterned lines using a JMONSEL-modeled library", Ultramicroscopy (2015), http://dx.doi.org/10.1016/j.ultramic.2015.01.004 .

[5] Brad Thiel, Michael Lercel, Benjamin Bunday, and Matt Malloy, "Assessing the Viability of Multi-Electron Beam Wafer Inspection for sub-20 nm Defects", Proc. SPIE 9236, Scanning Microscopies 2014, 92360E (2014); doi:10.1117/12.2069302.

[6] Villarrubia, J. S. , Ritchie, N. W. M., and Lowney, J. R. "Monte Carlo modeling of secondary electron imaging in three dimensions," *Proc. SPIE* **6518**, 65180K (2007).

[7] J. R. Lowney, A. E. Vladár, and M. T. Postek, "High-accuracy critical-dimension metrology using a scanning electron microscope," Proc. SPIE 2725, pp. 515-526 (1996); J. R. Lowney, "Application of Monte Carlo simulations to critical dimension metrology in a scanning electron microscope," Scanning Microscopy 10, pp. 667-678 (1996).

[8] J. S. Villarrubia and Z. J. Ding, "Sensitivity of SEM width measurements to model assumptions," Proc. SPIE 7272 (2009).

[9] Villarrubia, J. S., and Ding, Z. J. "Sensitivity of SEM width measurements to model assumptions," *J. Micro/Nanolith. MEMS MOEMS* **8**, 033003 (2009).

[10] Aron Cepler, Benjamin Bunday, Bradley Thiel, John Villarrubia. "Scanning electron microscopy imaging of ultra-high aspect ratio hole features". Metrology, Inspection, and Process Control for Microlithography XXVI. Proceedings of the SPIE, Volume 8324, pp. 83241N-83241N-14 (2012).

[11] J.S. Villarrubia, A.E.Vladár, B.Ming, R.J.Kline, D.F.Sunday, J.S.Chawla, and S.List, "Scanning electron microscope measurement of width and shape of 10 nm patterned lines using a JMONSEL-modeled library," Ultramicroscopy 154 (2015) 15. http://dx.doi.org/10.1016/j.ultramic.2015.01.004
[12] Bunday, Benjamin D. "Noise fidelity in SEM simulation". Proc. SPIE, Volume 11325, Metrology, Inspection, and Process Control for Microlithography XXXIV; 113250R (2020). https://doi.org/10.1117/12.2559631
[13] Bunday, B., Mukhtar, M., Quoi, K., Thiel, B., and Malloy, M. "Simulating Massively Parallel Electron Beam Inspection for sub-20 nm Defects". Proceedings of SPIE Vol. 9424, 94240J (2015).
[14] Benjamin Bunday, Abner Bello, Eric Solecky & Alok Vaid, "7/5 nm logic manufacturing capabilities and requirements of metrology", Proc. SPIE 10585, Metrology, Inspection, and Process Control for Microlithography XXXII, 105850I (22 March 2018); doi: 10.1117/12.2296679
[15] Maseeh Mukhtar, Benjamin Bunday, Kathy Quoi, Matt Malloy & Brad Thiel. "Measuring multielectron beam imaging fidelity with a signal-to-noise ratio analysis", J. Micro/Nanolith. MEMS MOEMS 15(3) 034004 doi: 10.1117/1.JMM.15.3.034004, Published in: Journal of Micro/Nanolithography, MEMS, and MOEMS Volume 15, Issue 3 (23 August 2016).
[16] Aron Cepler, Benjamin Bunday, Bradley Thiel &John Villarrubia. "Scanning electron microscopy imaging of ultra-high aspect ratio hole features". Metrology, Inspection, and Process Control for Microlithography XXVI. Proceedings of the SPIE, Volume 8324, pp. 83241N-83241N-14 (2012).
[17] Thiel, B., Mukhtar, M., Quoi, K., Bunday, B., & Malloy, M. (2016). "Patterned Wafer Inspection with Multi-beam SEM Technology", Microscopy and Microanalysis, 22(S3), 586-587. doi:10.1017/S1431927616003780
[18] Benjamin Bunday, Maseeh Mukhtar, Kathryn Quoi, Bradley Thiel, & Matt Malloy. "Simulating Massively Parallel Electron Beam Inspection for sub-20 nm Defects". Proceedings of SPIE Vol. 9424, 94240J (2015).
[19] J. S. Villarrubia, "Model validation for scanning electron microscopy", Proc. SPIE 12496-26 (2023, publishing pending).
[20] See details on Blender at website: https://www.blender.org/.